IEEE Access
Multidisciplinary | Rapid Review | Open Access Journal

Received November 7, 2019, accepted December 16, 2019, date of publication December 27, 2019,
date of current version January 6, 2020.

Digital Object Identifier 10.1109/ACCESS.2019.2962710

Passive Magnetic Localization Based on Connotative Pre-Calibration for Tongue-Machine-Interface

HUI-MIN SHEN[1,2], (Member, IEEE), DI GE[1], CHONG LIAN[1], AND YANG YUE[1]
[1]School of Mechanical Engineering, University of Shanghai for Science and Technology, Shanghai 200093, China
[2]State Key Laboratory of Fluid Power and Mechatronic Systems, School of Mechanical Engineering, Zhejiang University, Hangzhou 310027, China

Corresponding author: Hui-Min Shen (hmshen@usst.edu.cn)

This work was supported in part by the National Natural Science Foundation of China under Grant 51605291, and in part by the Open Foundation of the State Key Laboratory of Fluid Power and Mechatronic Systems under Grant GZKF-201806.

ABSTRACT In human-machine-interface study, recognition of conscious human motion by contactless passive magnetic marked method can provide abundant information, such as PM marked tongue-machine-interface (TMI). However, solution of this nonlinear magnetic inverse problem heavily relies on initialization. This paper takes advantage of the motion characteristics constrained by physiological structure, and develops an enhanced algorithm for real-time full-pose passive magnetic localization in TMI application. In the proposed algorithm, a predetermined-discretized database is introduced, and provides reliable initializations for the nonlinear magnetic localization problem. This database presents the connotative relationships between the location and orientation of passive magnetic source, termed location-orientation mapping database (LOMD). The influence of initialization and LOMD constitution on solving the nonlinear inverse magnetic problem are studied through extensive simulations. Test bench evaluations are conducted on the designed experiment system. The experiment results show that about 38.5 % localization improvement can be achieved with a real-time tracking frequency up to 56.5 Hz.

INDEX TERMS Magnetic localization, magnetic dipole, non-linear optimization, tongue-machine-interface.

I. INTRODUCTION

In diagnose of physical motor function disorder related to organs or tissues, such as limb, finger or tongue, accurate motion monitoring can provide important information for treatment. For instance, capture of tongue kinematics [1] provides a proper way to study and evaluate diseases related to motor speech disorders, such as dysarthria [2] or dysphagia [3]. During the stroke rehabilitation treatment, it has been proved that the plasticity of corticospinal system is greatly affected by motor trainings [4], [5]. Specifically, finger motion tracking during the rehabilitation treatment can provide quantifiable evaluation for treatment effect and reliability criterion for phase judgement [6], [7]. Besides, physical motor tracking can create a basis for developing an efficient interface between individuals who lost self-care abilities and the environment [8], [9], such as hand trajectory gesture recognition [10] or tongue-machine-interface (TMI) [11], [12] for potentially environment control. Compared with other non-contact tracking technologies [13], such as optical sensing or ultrasonic sensing, the noninvasive magnetic tracking begins to attract the interests of researchers in medicine applications recently [14, 15], taking advantages of similar magnetic permeability of human body with the free space and high safety without side-effects or biomechanical reaction.

The passive permanent magnet (PM) based magnetic tracking method can provide higher excited magnetic fields in a smaller form-factor than electromagnetic source without requirement for power supply. All of these features make it more suitable to perform tracking task in short-distance medicine applications [14]. With the help of magnetic sensing system, immediate magnetic field distribution (MFD) on the position monitored by sensor can be known, which is mixture of MFD from the marked PM and environment noise. In recent years, successful tongue motion tracking has been applied in cursor control [16], text typing [17], [18] or mobile device navigating [19], [20] by attaching a magnet or ferromagnetic marker on the apex of the tongue,

The associate editor coordinating the review of this manuscript and approving it for publication was Zhixiong Peter Li.

and both intraorally and out orally. However, limited feature commands are classified from the measured MFD signals and utilized in these researches.

Directly computing the PM location and orientation with magnetic sensing system measurements and formulated forward MFD model, referred to as inverse magnetic problem solving [21]. This can provide intuitive control signals, where the suppleness and flexibility of the tongue can be fully exploited. However, due to the ill-posedness and nonlinearity of this inverse problem, time-consuming iterative algorithms, redundant measurements and reliable initializations are always required [22], [23].

With the increasing requirements in high-accurate localization for real-time medicine applications, various methods focused on improvements in sensing system and algorithm have been developed to solve the nonlinear inverse problem. In [24], a grid-based sensor layout optimization method was presented for fixed sensor number and defined distribution area. An 8 × 8 2-D single axial sensing array was developed for real-time magnetically manipulated untethered robot localization in [25]. Generally, more sensors can provide better accuracy, but redundant measurements will take more computational time.

Strategies focused on improvements of the nonlinear inverse model could provide solutions with low computation. Song *et al.* [26] established a closed-form analytical model for an annular magnet based on the Biot-Savart Law and solved the inverse magnetic problem by particle swarm optimization algorithm. In [22], Hu *et al.* presented a linear algorithm by the matrix and algebra computations to localize a magnetic dipole according to the co-planarity among the magnetic field at the measured point and the dipole's position and orientation parameters. In our previous study [27], a closed-form analytical inverse model was proposed by introducing a PM-upright device. Di *et al.* [28] defined a closed-form expression for the Jacobian of the magnetic field relative to the tracked target, and realized real-time localization with an alternative algorithm fusing inertial measurements. Improvements in the forward model of PM are also studied, such as distributed multilevel current model [29] and set of partial differential equations [30].

Although, magnetic localization technologies for medical applications are emerging, those researches focused on tissue and organ motion tracking are limited. In particular, the motion characteristics constrained by physiological structure is rarely considered in these researches. Besides, due to the attenuation characteristic of magnetic field with distance in passive magnetic system, the sensing systems are always bulky. In [31], we established a location-orientation mapping database based on restricted kinematic property of target motion for magnetic localization, and validated the effectiveness of the proposed algorithm by simulations. This paper presents an enhanced algorithm for real-time full-pose passive magnetic localization for TMI, combining the self-restriction that the motion of tissue and organ is muscular-skeletally restricted. This paper is organized as follows:

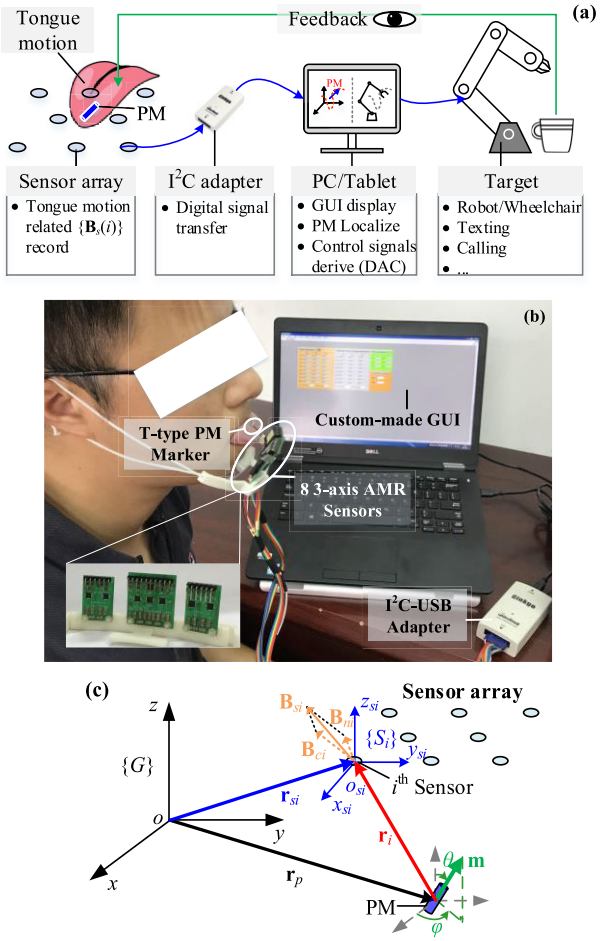

FIGURE 1. Scheme illustrates passive PM localization in TMI system. (a) Illustration of PM marked TMI system; (b) The system architecture of previously proposed TMI [9]; (c) Localization system with PM maker modeled as a magnetic dipole.

- Section II presents the methodology, including the system architecture of the proposed magnetic marked TMI, inverse magnetic localization model, MFD sensitivity to position parameters (location and orientation), and establishment of proposed Location Orientation Mapping Database (LOMD);
- Section III introduces the experiment system;
- In Section IV, MFD sensitivity to position parameters, and the influence of initialization and LOMD constitution on solving the nonlinear magnetic problem are studied through extensive simulations;
- In Section V, test bench evaluations are carried out on the experiment system;
- Section VI concludes the study of this paper.

II. METHODOLOGY

In magnetic tracking application for tissue and organ motion monitoring, a passive magnetic source, normally a PM, is attached to the tracked target, such as tongue ape in TMI system. Then, the PM motion can represent conscious tongue movement.

A. SYSTEM ARCHITECTURE OF THE PROPOSED MAGNETIC MARKED TMI

For a passive PM marked TMI system illustrated in Figure 1(a), the derived space MFD at the known observation points can be measured by magnetic sensor array and transferred to PC/tablet through a communication interface, such as I^2C to USB adapter employed in this paper. Then, real-time PM localization can be provided by processing sensor measurements with algorithm loaded on the PC/tablet. Accordingly, control signals can be derived based on tracked PM motion intentionally driven by tongue. Finally, disabled individuals can control a robot to have a drink or text their families through a graphic-user-interface (GUI) established on the PC/tablet.

In our previous study, a proof-of-concept prototype TMI system utilizing a combined T-type PM marker for potentially environment control was introduced. As presented in Figure 1(b), a T-type PM marker is employed for tongue motion tracking, whose magnetic fields are measured by an anisotropic magnetoresistive (AMR) sensor array fixed on a mask produced with 3-D printing technology. Then, the trajectory of the marked tongue position can be figured out and presented by a custom-made GUI based on LABVIEW and MATLAB loaded on PC.

B. INVERSE MAGNETIC MODEL

If the main dimension of the magnetic source is smaller than one fifth of its distance to the observed point, the magnetic source can be modeled as a magnetic dipole in Figure 1(c). Based on the premise of magnetic dipole model, the magnetic fields at sensor observation point o_{si} (whose local coordinate is represented by $\{S_i\}$) $\mathbf{B}_{ci} = [B_{xi}, B_{yi}, B_{zi}]^{\mathrm{T}}$ from the PM can be formulated by

$$\mathbf{B}_{ci}\left(\mathbf{r}_p, \mathbf{m}\right) = \left[B_{xi} \;\; B_{yi} \;\; B_{zi}\right]^{\mathrm{T}} = \frac{\mu_0 m}{4\pi} \frac{3\left(\mathbf{m} \bullet \mathbf{n}_i\right)\mathbf{n}_i - \mathbf{m}}{r_i^3} \tag{1a}$$

$$\mathbf{r}_i = r_i \mathbf{n}_i = \mathbf{r}_{si} - \mathbf{r}_p \tag{1b}$$

where μ_0 is the permeability of human tissue, which approximates to the air permeability ($=4\pi \times 10^{-7}\mathrm{N/A}^2$); r_i and $\mathbf{n}_i$ is the magnitude and unit vector of distance vector $\mathbf{r}_i$ pointing from PM location vector $\mathbf{r}_p$ to a fixed sensor location vector $\mathbf{r}_{si}$, respectively; $\mathbf{m}$ is the unit orientation vector with the polar parameters θ and φ in global coordinate $\{G\}$; m is magnitude of the magnetic dipole moment.

To derive the marked PM position parameters ($\mathbf{r}_p$, $\mathbf{m}$) in Figure 1(c), an inverse magnetic model in (2a) can be formulated according to the differences between the computed MFD $\mathbf{B}_{ci}$ from the forward model in (1) and measurements $\mathbf{B}_{si}$ of fixed sensor array. A least-square (LS) based inverse model is established, since the noise interference $\mathbf{B}_{ni}$ in (2b) can be eliminated in the hypothesis of white noise from the environment. Computation work brought by high-order characteristics of the forward model in (1) can also be reduced. The magnetic fields $\{\mathbf{B}_{si}\}$ can be measured by magnetic sensors at the known observation points $\{\mathbf{r}_{si}\}$, and utilized as known information to solve the inverse magnetic localization model and derive the position parameters.

$$f(\mathbf{r}_p, \mathbf{m}) = \sum_{i=1}^{N} \|\mathbf{B}_{si} - \mathbf{B}_{ci}\|^2 \tag{2a}$$

$$\mathbf{B}_{si} = \mathbf{B}_{ni} + \mathbf{B}_{ci} \tag{2b}$$

where $\mathbf{B}_{si}$ is observation of the i^{th} sensor; N is the total number of sensors in the sensor array; $\mathbf{B}_{ci}$ is theoretical MFD of the i^{th} sensor computed from the forward model in (1).

Solution to the magnetic localization problem in (2a) needs to find the optimal parameters ($\mathbf{r}_p$,$\mathbf{m}$) that minimize the objective function $f(\mathbf{r}_p, \mathbf{m})$, where nonlinear LS optimization techniques are always applied to get an optimized solution. Combining the global convergence of the steepest method and the quadratic convergence of Newton's method, the Levenberg-Marquardt algorithm (LMa) can provide good calculation accuracy with better robustness [32]. However, during the iteration process, the variation between each iteration step is greatly affected by the initializations. Large deviations or redundant iteration time-cost may be resulted if the initializations are far off the final minimum [33]. Here we try to provide more reliable initializations for the inverse problem, utilizing the restrictions between the localization and orientation parameters.

C. MFD SENSITIVITY TO POSITION PARAMETERS

Although location parameter $\mathbf{r}_p$ is the target to be monitored in magnetic tracking, both location and orientation are required to be solved in (2). This makes the number of initialization parameters increase from three parameters (x, y, z) to five parameters (x, y, z, θ, φ), which brings more challenge and computation work to solve the inverse magnetic problem. Considering that initializations play an important role in inverse magnetic problem solving, the individual impact of location and orientation initial values on the inverse problem is discussed firstly. It is reasonable to understand that if the location parameter, who has a greater influence on the inverse problem, can be provided by pre-calibration, then according to the motion characteristics constrained by physiological structure, corresponding initial orientation parameter with improved accuracy can be obtained. Then, improved accuracy of the inverse problem solution can be derived with the figured initializations.

We define sensitivity concept, which qualitatively describe the change of derived space MFD with change of location (x, y, z) and orientation (θ, φ), to illustrate location parameter and orientation parameter impact to inverse magnetic problem solving. Then, a discrete magnetic source location and orientation collection can be formulated by connotative pre-calibration, and the parameter set (location or orientation) with more sensitivity can be utilized to search for the other parameter set (orientation or location) correspondingly in real-time tracking. This will provide more reliable initialization with less computational workload.

Thus, sensitivity of magnetic source location and orientation parameters is assessed firstly. It is obvious in (2) that the MFD $\mathbf{B}_c$ generated by the magnetic dipole is inversely proportional to three times of the distance r between the dipole and observation point. Suppose that the observation point is located at the origin for simplicity, we can get the distance vector $\mathbf{r}= -\mathbf{r}_p$. For the same magnetic dipole, the gradient of the MFD $\mathbf{B}_c$ along the distance vector $\mathbf{r}$ can be written as

$$\begin{aligned}\nabla\mathbf{B}_c &= \left[\nabla B_x \;\; \nabla B_y \;\; \nabla B_z\right]^{\mathrm{T}} \cdot \mathbf{n}dr \\ &= \frac{\mu_0 m}{4\pi}\left[3\left(\mathbf{m}\bullet\mathbf{n}\right)\mathbf{n}-\mathbf{m}\right]\left(\frac{\partial}{\partial r}\frac{1}{r^3}\right)dr \end{aligned} \tag{3}$$

Then, an equation directly relating distance vector $\mathbf{r}= r\mathbf{n}$ to magnetic field measurement $[B_x \;\; B_y \;\; B_z]^{\mathrm{T}}$ and its spatial gradients at $\mathbf{r}$ (which is represented by $\nabla B_x = \left(\partial_x B_x \;\; \partial_x B_y \;\; \partial_x B_z\right)^{\mathrm{T}}$, $\nabla B_y = \left(\partial_y B_x \;\; \partial_y B_y \;\; \partial_y B_z\right)^{\mathrm{T}}$, $\nabla B_z = \left(\partial_z B_x \;\; \partial_z B_y \;\; \partial_z B_z\right)^{\mathrm{T}}$) can be derived by applying (2) into (3), from which the distance vector $\mathbf{r}$ can be solved.

$$\mathbf{r}=r\mathbf{n}=-3\left[\left(\nabla B_x \;\; \nabla B_y \;\; \nabla B_z\right)^{\mathrm{T}}\right]^{-1}\left[B_x \;\; B_y \;\; B_z\right]^{\mathrm{T}} \tag{4}$$

The direct relation between $\mathbf{r}$ $(= -\mathbf{r}_p)$ and MFD in (4) presents more sensitivity of location parameter $\mathbf{r}$ $(= -\mathbf{r}_p)$ to the MFD than orientation parameter $\mathbf{m}$. For general magnetic tracking, since the observed sensor location $\mathbf{r}_{si}$ is known, the distance vector $\mathbf{r}$ is determined by source location $\mathbf{r}_p$. Then, the location parameter is more sensible than orientation parameter to MFD measurements in forward model, and the accuracy of solved location parameter is better than orientation parameter in inverse problem solving. It can be inferred that the accuracy of the computed location parameter derived from the measured MFD is more than orientation parameter.

D. ESTABLISHMENT OF DISCRETIZED LOMD

To provide reliable initializations for the nonlinear magnetic localization problem, we construct a predetermined-discretized database. This database presents the connotative relationships between the location and orientation, termed LOMD. The LOMD is off-line predetermined and formed by a collection of the discretized localization for the tracked target by pre-sampling. Based on the physiological fact that the motion of tracked target, such as arthrosis or tongue, is muscular-skeletally restricted, it is feasible to assume that the location and orientation of the tracked target is corresponding and unique. Then, this database can be applied for tracking in the whole positioning region.

The discretized sample of the LOMD database is determined through multi-times of nonlinear optimization problem in (2a) solving, where mean value of the multi-time solutions is taken as final result. Although the final calibrated result is not ideal with some deviation, the error is acceptable. This kind of pre-calibration is time consuming, and not proper for in-time application. But, calibration of limited discretized sample in LOMD is a preferred choice.

The construction of the LOMD will affect the accuracy and efficiency of the proposed enhanced algorithm partly. High-density LOMD will require more computational time both in establishment and inverse computing. On the contrary, little improvement will be brought with sparse LOMD distribution. Since the trajectory of the target is unknown during localization, establishment of LOMD with homogenous density is advisable, which is illustrated as follows.

1) **S1.** Positioning region determination: Sporadic positions of the target motion are located and figured out by traditional LMa. The smallest cube encloses the limit positions is assumed to be the positioning region.
2) **S2.** Uniform division of the positioning region: Since the location parameter get more attention in the magnetic tracking technologies, we divide the space of the figured positioning region by equal distance Δd, generating an array of uniformly distributed nodes. The interval Δd $(= k\bar{t}\cdot v)$ is determined by the mean processing time $\bar{t}$ spent on solving the inverse magnetic problem once utilizing traditional LMa with random initializations, the movement speed v, and a weight coefficient k.
3) **S3.** LOMD Determination: The MFDs on the sensors are sampled by moving the tracked target to the nodes determined in **S2**. We will keep it blank, if the tracked target cannot reach the node. Then, the location and orientation parameters of the nodes can be determined by traditional LMa with initializations of $\mathbf{r}_{p0} = (x_p(B_{s\_max}), y_p(B_{s\_max}),$ random $z_p)$ and $\mathbf{m}_0 =$ random (θ, φ) for 1000 times, and the mean value for each node construct the final LOMD for on-line tracking.

This predetermined off-line LOMD can provide corresponding location and orientation parameters. Then, in real-time tracking the initial orientation parameter can be provided according to solved location parameter with improved accuracy in LOMD. This will facilitate magnetic tracking with high accuracy and efficiency.

E. ALGORITHM WITH ENHANCED INITIALIZATION PROVIDED BY LOMD

A novel magnetic localization algorithm is devised based on the LOMD for solving the high order 5-D inverse problem in (2), and the computational flowchart is presented in Figure 2. In the proposed inverse localization process, a preliminarily determined localization result, including location and orientation parameters, is obtained from the 1st step with rough convergence conditions. Then, in the 2nd step a set of enhanced localization initialization with more accuracy can be deduced according to the preliminarily determined location parameter from the LOMD, taking account that the location is more sensitive to the change of MFD. Thereafter, the 3rd step of the inverse localization process executes with the deduced initialization and the same rough convergence conditions, and provides the final localization result.

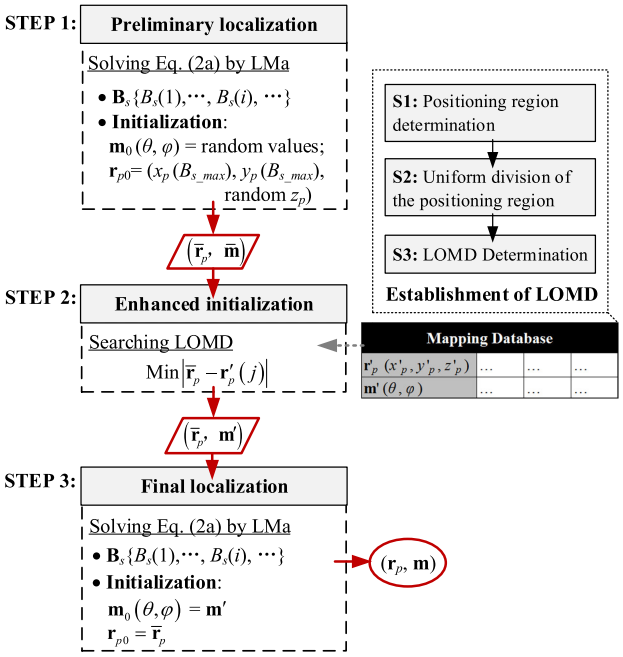

FIGURE 2. Flowchart of proposed enhanced magnetic localization algorithm based on LOMD.

To be specific, three steps are involved:

- **Step 1 Preliminary localization:** With the real-time measurements, specific initializations ($\mathbf{r}_{p0}$, $\mathbf{m}_0$) and rough tolerance are provided. Based on the plane distributed sensor array and the attenuation relationship between the MFD and distance, we assign $\mathbf{r}_{p0}$ = ($x_p(\mathbf{B}_{s\_max})$, $y_p(\mathbf{B}_{s\_max})$, random z_p) and $\mathbf{m}_0$ = random (θ, φ), where $x_p(\mathbf{B}_{s\_max})$ and $y_p(\mathbf{B}_{s\_max})$ are the xy-plane location of the sensor with the strongest measurement. A pre-estimated localization result $(\bar{\mathbf{r}}_p, \bar{\mathbf{m}})$ can be derived by solving (2a) with ($\mathbf{r}_{p0}$, $\mathbf{m}_0$).
- **Step 2 Enhanced initialization:** Based on the different sensitivities of location and orientation to the MFD, the pre-estimated location result $\bar{\mathbf{r}}_p$ in **Step 1** is employed for enhanced orientation searching in LOMD. The location parameter $\mathbf{r}'_p$ closest to $\bar{\mathbf{r}}_p$ in the LOMD is figured out. Then, an enhanced orientation $\mathbf{m}'$ can be determined, which is corresponding with the location $\mathbf{r}'_p$ in the LOMD. $(\bar{\mathbf{r}}_p, \mathbf{m}')$ will be utilized as initialization in the next step.
- **Step 3 Final localization:** Given the initialization $(\bar{\mathbf{r}}_p, \mathbf{m}')$ derived from the former step, the solving process of the inverse problem in the 2nd round speeds up and provides improved final solutions ($\mathbf{r}_p$, $\mathbf{m}$).

The introduction of the LOMD can provide initialization with more accuracy, and facilitate the inverse localization result with the proposed enhanced algorithm.

III. EXPERIMENT SYSTEM

Experiments were conducted on a developed system to validate the feasibility and availability of the proposed magnetic localization method based on the enhanced algorithm combining the LOMD. The experiment system consists of tongue motion simulation mechanism, data acquisition part and human-machine interface (HMI) as illustrated in Figure 3. In the following study, analyses and discussions on location accuracy are conducted.

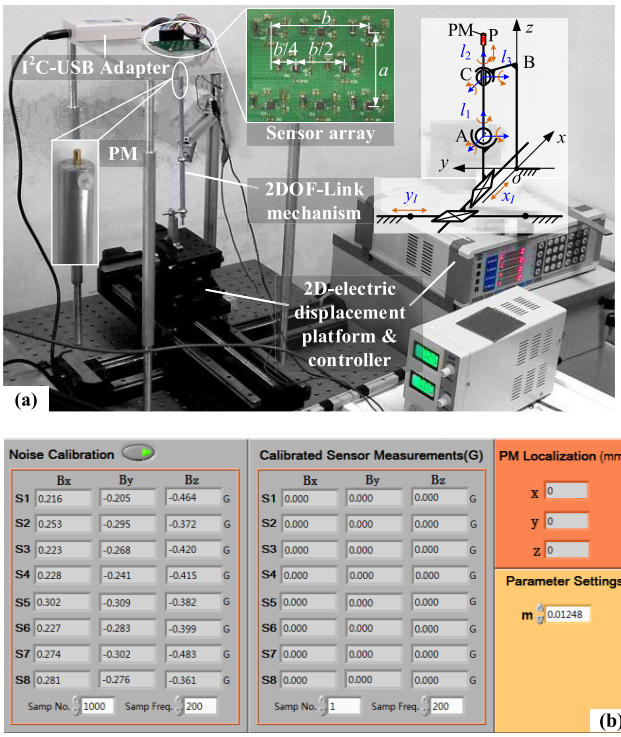

FIGURE 3. The designed experiment system. (a) Experiment setup; (b) Graphical user interface (GUI).

A. TONGUE MOTION SIMULATION MECHANISM

To evaluate the feasibility and effectiveness of the proposed magnetic localization algorithm, calibrated test bench should be established. However, the tongue motion is limited in the sealed intraoral region. It is impossible to vividly calibrate tongue apex motion in real-time. Based on possible motion tracks of the tongue apex, we developed a linkage mechanism to partly simulate human tongue apex movement.

As illustrated in the upper right corner of Figure 3(a), point P represents the tongue apex, where is attached a PM. This linkage mechanism is driven by a 2-D electric linear stages (Winner Optic®WN02RA-230TA, resolution: 5 μm) with controller (Winner Optic®WNMPC2810), and can provide well-defined 2-DOF motion, since the number of driving components is the same with that of mechanism freedom. Therefore, the PM motion trajectory ($\mathbf{r}_p$, $\mathbf{m}$) can be determined by the designed mechanism parameters, including link length l_1 (= 90.0 mm), l_2 (= 154.0 mm) and l_3 (= 318.2 mm), and linear stage inputs (x_I, y_I):

$$\begin{cases} x_P = (1+w)\dfrac{\sqrt{2}}{2} l_3 - w x_I \\ y_P = (1+w)\dfrac{\sqrt{2}}{2} l_3 - w y_I \\ z_P = (l_1 + l_2)\cos\theta \end{cases} \tag{5a}$$

$$\mathbf{M}:\begin{cases}\theta = \arcsin\dfrac{\sqrt{\left(2x_I-\sqrt{2}\,l_3\right)^2+\left(2y_I-\sqrt{2}\,l_3\right)^2}}{2l_1}; \\ \quad \theta\in\left[0,\pi/18\right] \\ \varphi = k\pi - \arctan\left(\dfrac{2y_I-\sqrt{2}\,l_3}{\sqrt{2}\,l_3-2x_I}\right); \\ \quad \varphi\in[0,2\pi] \\ \text{where } k=\begin{cases}0, & \text{if}\sqrt{2}y_I\le l_3\&\sqrt{2}x_I\le l_3\\ 1, & \text{if}\sqrt{2}x_I\ge l_3\\ 2, & \text{if}\sqrt{2}y_I\ge l_3\&\sqrt{2}x_I\le l_3\end{cases}\end{cases} \tag{5b}$$

where $w = l_2/l_1$; $\theta \in (0°, 10°)$ since the range of the pendulum angle of the selected ball bearing (STRUENING®, LTLM5R) is 20°.

Theoretically, the PM motion can be restricted and pre-calibrated inside a space the same with oral cavity, about left-to-right 60 mm, front-to-back 30 mm, and top-to-bottom 50 mm. However, since the simulated tongue apex motion is driven by the developed linkage mechanism, its motion will be limited by the ball bearing rotation angle. The simulated tongue apex motion is distributed on a spherical cap of a spherical cone with spherical radius $r = l_2$ and zenith angle $\theta = 10°$ centered at point C in Figure 3(a). The PM motion range on the xy-plane is a circle with a radius of 26 mm.

B. SENSING SYSTEM

As presented in Figure 3(a), a cylindrical NdFeB magnet is used as magnetic marker (Φ1.6 mm × 6.5 mm, Br = 0.1430 T, m = 0.0125± 0.0001 A·m^2), which is magnetized along longitudinal axis. We built a plan (a = 30.0 mm, b = 40.0 mm) distributed sensor array consisting 8 channel 3-axis sensors (Honeywell®, HMC5983, resolution: 0.227 μT, range: ±0.4 mT, maximum output rate: 220 Hz) for magnetic field measurements. The magnetic field data was transferred to PC (i7-6600U CPU, 16GB RAM, DELL/Latitude®) by a 12-bit I^{2}C-to-USB adapter (Viewtool®).

C. HUMAN-MACHINE INTERFACE

Dedicated HMI is developed based on LABVIEW (2014, NI®) and MATLAB (R2014a, MathWorks ®) loaded on PC. Figure 3(b) presents the GUI for sensing data process and information display. The *Noise Calibration* presents the noise level on the sensor position before the PM marker is mounted, based on the assumption that the noise level at the sensor observation point is constant. The *Calibrated Sensor Measurements* displays the sampled MFDs on each sensor channel, including sample number and frequency information. The *PM Localization* provides the optimization results processed by the proposed enhanced magnetic localization algorithm based on LOMD through MATLAB. The *Parameter Settings* presents the magnetic moment magnitude m of PM marker, which is pre-calibrated by Gauss-meter (Lakeshore®421, resolution: 0.1 μT).

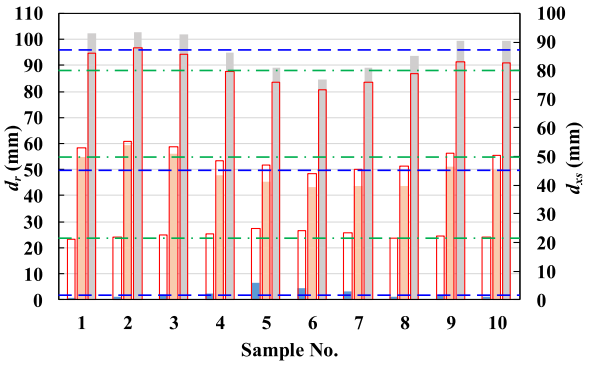

FIGURE 4. Comparison of the mean localization error d_r (colored bar) and the mean initial guess error d_{xs} (transparent bar).

IV. SIMULATION STUDY OF LOMD PERFORMANCE

Before test bench evaluation, MFD sensitivity to position parameters, and the influence of initialization and LOMD constitution on solving the nonlinear magnetic problem in (2) are studied through extensive simulations. The programs are processed by MATLAB on PC.

A. INITIALIZATION INFLUENCE ON NONLINEAR OPTIMIZATION ALGORITHM

In the aforementioned section, it is supposed that LMa may fail to give correct solution, if the initial guess of the unknown parameters were far from the correct solution. Before test bench evaluation, the influence of initial guess to the traditional LMa processing is studied through simulation. Localizations of 10 target positions, whose locations on the xy-plane distributed along the diagonal line of the motion region in Figure 3(a) are discussed. The distance between the true position parameters for each discussed point and the initial guess value is divided into three guess error intervals, including [0, 30] mm, [30, 60] mm, and [60, 90] mm. Then, 1000 sets of initial guesses, which are randomly distributed in each interval are generated, are utilized to solve this inverse problem by LMa. The guess of unit orientation vector is stochastically for all location initial guesses. Totally, 30 000 sets of initial guesses are evaluated. Noise-free sensor measurements according to forward model in (1) are utilized to solve this inverse problem in initial guess evaluation, to reduce the impact of measurements quality on localization.

For each initial guess interval, the mean localization error d_r (distance between the solved location $\mathbf{r}_{pm}$ and true location $\mathbf{r}_{pc}$, marked by colored bar) and the mean initial guess error d_{xs} (distance between the initial guess $\mathbf{r}_{p0}$ and true location$\mathbf{r}_{pc}$, marked by transparent bar) for each position are displayed on the left and right y-axis respectively in Figure 4. When the initial guess distributed in the interval with the smallest mean guess error, the mean localization error d_r solved by LMa with 10 000 sets of initial guesses is distributed between [0.65, 6.48] mm with a mean value of 2.37 mm for all 10 discussed tracking positions. For the

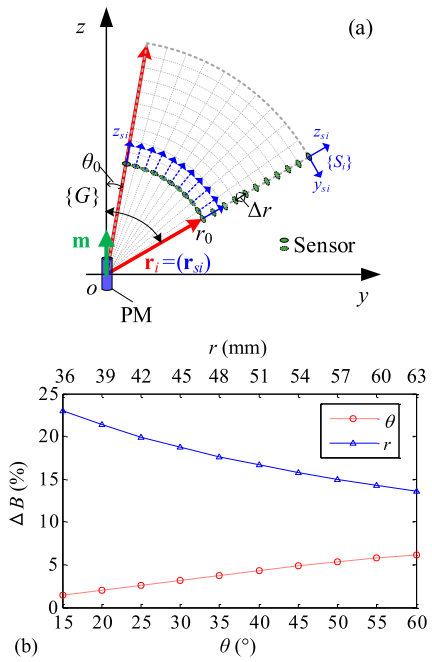

FIGURE 5. Effects of location parameter and orientation parameter on the space MFD derived from the magnetic source. (a) Observation point illustration; (b) Comparison of the magnitude change rate ΔB of the adjacent observation point.

other two guess error intervals, the mean localization error d_r is 49.47 mm and 95.70 mm, respectively.

As presented by green dots line in Figure 4, the mean guess error for each interval is 22.64 mm, 49.48 mm and 80.89 mm, respectively. However, the mean localization error based on each initial guess interval varies dramatically from 2.37 mm to 49.47 mm and 95.70 mm, as shown by the dashed blue lines in Figure 4. The mean localization error (49.47 mm) is almost in the same level for interval [30, 60] mm with a mean guess error (49.48 mm). The impact of initial guess increases for interval [60, 90] mm, since the mean localization error (95.70 mm) is even larger than the mean guess error (80.89 mm). The rapid increase of localization error with initial guess errors implies the significant impact of initial guess for nonlinear optimization algorithm.

B. MFD SENSITIVITY ASSESSMENT TO POSITION PARAMETERS

To quantitatively illustrate the different effects of location parameter and orientation parameter on the space MFD derived from the magnetic source, simulations were carried out and presented in Figure 5. As presented by Figure 5(a), it is supposed that the magnetic target is located on the origin o of the global coordinate $\{G\}$, and its magnetic moment is coinciding with the z-axis. The observation points are distributed on the yz-plane, where the space MFD are analyzed. The sensing axis z_{si} of the i^{th} sensor is kept to along the radial direction of polar coordinate, while the radius r and polar angle θ of the observing sensor location change. The start sensor location is $r_0 = 33$ mm (satisfy premise of magnetic dipole that main dimension of the magnetic source is smaller than one fifth of its distance to the observed point), $\theta_0 = 10°$, and $\varphi_0 = 0°$ (keep constant). Then, the radius changes by $\Delta r = 3$ mm (rate of change is 10%), and the polar angle θ changes by $\Delta\theta = 5°$ (rate of change is 50%), individually. As illustrated in Figure 5(a), 11 samples are discussed for each condition, and totally 21 samples are involved.

The simulated MFD on the aforementioned observation points were computed according to (1), and the magnitude change rate ΔB of the adjacent observation point were compared in Figure 5(b). The red dashed line with circle marker in Figure 5(b) displays ΔB changes from $\theta_0 = 10°$ to 60° with constant radius r_0. The blue solid line with triangular marker presents ΔB changes from $r_0 = 33$ mm to 63 mm with constant polar angle $\theta = 60°$. The comparison results show that:

- ΔB decreases from 22.9% to 13.6% with the radius r variation from 36 mm to 63 mm.
- While ΔB increases from 1.4% to 6.2 % with polar angle θ variation from 15 ° to 60 °.
- Although, the change of polar angle is much larger, the change of MFD caused by distance variation is more significant.

For general magnetic tracking, since the observed sensor location $\mathbf{r}_{si}$ is known, the distance vector $\mathbf{r}_i$ is determined by source location $\mathbf{r}_p$. Then, the location parameter is more sensible than orientation parameter to MFD measurements in forward model, and the accuracy of solved location parameter is better than orientation parameter in inverse problem solving. It can be inferred that the accuracy of the computed location parameter derived from the measured MFD is more than orientation parameter.

C. LOMD ASSESSMENT

The LOMD for magnetic localization algorithm is determined through off-line calibration as follows.

- **S1.** Positioning region determination: the PM movement is controlled by 2-D electric displacement platform, restricted on spherical cap of a spherical cone with spherical radius $r = l_2$ and zenith angle $\theta = 10°$ centered at point C in Figure 3(a). The PM motion range on the xy-plane is a circle of radius 26 mm.
- **S2.** Uniform division of the positioning region: to determine the division interval $\Delta d\ (= k\bar{t} \cdot v)$, the mean computational time $\bar{t}$ spent on solving the inverse magnetic problem once utilizing traditional LMa with random initializations is figured out through 1000 trials. We got $\bar{t} =$ 27.2 ms with a standard deviation of 3.8 ms. Besides, it has been reported that tongue movement speed during swallowing and speech changes within 2.10 $\sim$ 32.43 mm/s. Thus, we take the movement speed $v =$ 30 mm/s. The positioning region is uniformly divided along polar angles according to the arc length determined by Δd.

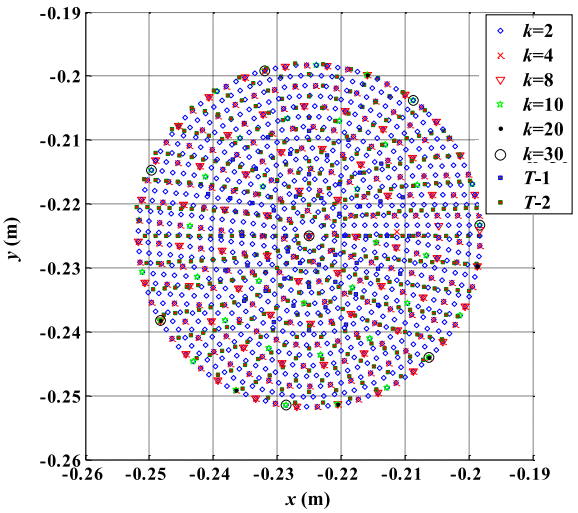

FIGURE 6. Nodes distribution on the *xy*-plane for each LOMD constructed with various k and traces T-1 & T-2 to be estimated in simulation.

TABLE 1. Constructed LOMD.

k	2	4	8	10	20	30
Node No.	901	238	67	44	11	8
Δd (mm)	1.632	3.264	6.528	8.16	16.32	22.48

- **S3.** LOMD Determination: With determined division interval Δd in **S2**, the location and orientation parameters of the nodes in LOMD are determined by traditional LMa with initializations of $\mathbf{r}_{p0} = (x_{si}(\max \mathbf{B}_{si}), y_{si}(\max \mathbf{B}_{si}),$ random $z_p)$ and $\mathbf{m}_{p0} =$ random (θ, φ) for 1000 times. To assess the density and quality of LOMD on PM localization, constructions of LOMD with integer weight coefficients k and SNR levels (2, 5, 10, 20, 50) defined by (6) are performed.

$$\mathrm{SNR} = \left(\sum_{i=1}^{N} B_{ci}^2\right) / \left(\sum_{i=1}^{N} B_{mi}^2\right) \tag{6}$$

The ambient noise is assumed to be Gaussian white noise.

The node number with division interval Δd for each LOMD of various weight coefficient k is presented in Table 1. The node distribution on the xy-plane is displayed in Figure 6. To investigate the influence of different LOMD distributions and qualities on localization performance, simulations were carried out. Two damped helix traces (termed T-1 and T-2) are designed for evaluation, as illustrated in Figure 6 marked by blue and red colored squares. The radius varies from 3.8 mm to 17.1 mm for T-1 and from 1.9 mm to 27.4 mm for T-2.

Firstly, simulations were carried out to investigate the influence of measurements SNR levels on calibrated LOMD quality. Based on the forward model in (1) and SNR model in (6), the sensor array measurements under different SNR levels while the PM located on each node of the LOMD can be achieved. Then, the LOMD nodes can be located by solving the inverse model in (2) with simulated measurements of different SNR levels. Figure 7 presents the mean localization error e_r of computed LOMD localizations with various weight coefficient k solving by LMa with simulated sensor measurements under different SNR levels. Totally, 1000 groups of simulations for each k and SNR level were carried out.

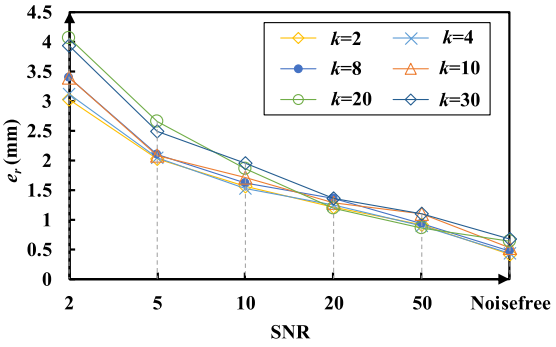

FIGURE 7. Computed LOMD localization error e_r with various weight coefficient k under different SNR levels.

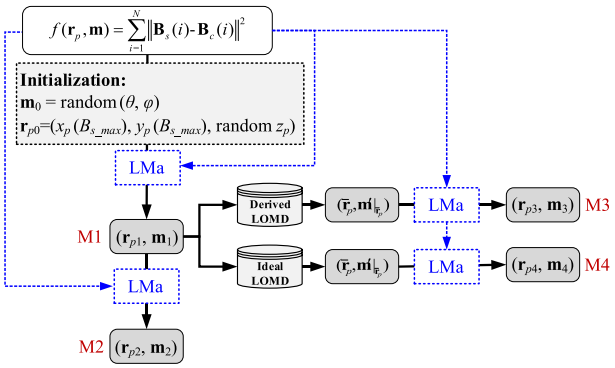

FIGURE 8. Flowchart comparison of four methods for magnetic localization.

It is obvious that the overall mean localization accuracy of LOMD in Figure 7 gets better with the increase of SNR levels. The mean localization errors of sparse node distributions are more significant. This gets apparent at low SNR levels. When SNR=2, e_r of $k = 20$ and $k = 30$ are about 30 % higher than the others.

Localization performances of four methods are quantitatively compared by

$$\varepsilon_i(\%) = (e_{r1} - e_{ri})/e_{r1} \times 100\% \tag{7}$$

where e_{r1} is the mean localization error derived by M1; e_{ri} is the mean localization error derived by Mi($i = 2$, 3 and 4). The algorithm flowcharts are illustrated in Figure 8, including:

- **M1**: solving (2) by traditional LMa with initialization of $\mathbf{r}_{p0} = (x_{si}(\max \mathbf{B}_{si}), y_{si}(\max \mathbf{B}_{si}),$ random $z_p)$ and $\mathbf{m}_{p0} =$ random (θ, φ), whose results are presented by $(\mathbf{r}_{p1}, \mathbf{m}_{p1})$ and assessed by e_{r1}.

- **M2**: solving (2) by traditional LMa taking $(\mathbf{r}_{p1}, \mathbf{m}_{p1})$ as initialization, whose results are presented by $(\mathbf{r}_{p2}, \mathbf{m}_{p2})$ and assessed by e_{r2} and ε_2.
- **M3**: solving (2) by the proposed magnetic localization algorithm with computed LOMD derived from sensor measurements, whose results are presented by $(\mathbf{r}_{p3}, \mathbf{m}_{p3})$ and assessed by e_{r3} and ε_3.
- **M4**: solving (2) by the proposed magnetic localization algorithm with true LOMD, whose results are presented by $(\mathbf{r}_{p4}, \mathbf{m}_{p4})$ and assessed by e_{r4} and ε_4.

For each damped helix trace, 1000 groups of simulations are performed with different k of calibrated LOMD and SNR levels. In method M3 processing, the derived LOMD is calibrated from measurements containing noise of the same SNR level with that utilized for trace localization. In method M4 processing, ideal LOMD is constructed according to the linkage mechanism model in (5). The mean localization error e_r for each method, and the improvement ratio ε compared with M1 for methods M2 and M3 are presented in Figure 9.

The mean localization errors for each method in Figures 9(a) and (c) show that, although LMa is also performed twice in method M2, e_{r3} and e_{r4} are smaller than e_{r1} and e_{r2} for both trace tracking. Besides, the localization error derived by M3 is close to that of M4 for the same level with different node density, verifying the improvement brought by LOMD no matter pre-calibrated (M3) or ideal (M4). In Figures 9(b) and (d), the improvement ratio of M3 ($k = 30$) at SNR=2 is 19% and 13% in T-1 and T-2 respectively, which is about twice of that for M2. This verifies that without the benefit brought by pre-calibrated LOMD on initial guess, improvement of simply LMa repeat processing is limited.

The difference of the localization error in M4 (ideal LOMD, where noise impact on LOMD can be ignored) between LOMD with sparse node density ($k = 20$ and 30) and larger node density ($k = 2$, 4, 8 and 10) gets apparent with SNR level increase in Figures 9(a) and (b). Implying that, the LOMD node density has an impact on localization performance, and this impact becomes obvious with SNR levels increase. However, the results are almost the same for $k = 2$, 4, 8 and 10, implying that the improvement of LOMD node density increase is limited. Combined the results in Figure 9, we take the weight coefficient k equals 10.

Comparisons of Figures 9(b) and (d) show that, the localization improvement ratio of M3 with derived LOMD of sparse node density is about the same level or even a little better than that with larger node density. This is mainly due to inaccuracy of LOMD calibrated from noised measurements, whose impact expands with density increase. However, ε_3 is still much better than ε_2 at all SNR levels.

To evaluate the cost on processing time, we analyzed the mean time spent on two trajectories localization by methods M1, M2 and M3. The processing time increase ratio Δt (%) of Methods M2 and M3 compared with that of M1 is displayed in Figure 10. Although LMa is implemented twice in both algorithms M2 and M3, the time increase ratio Δt_2

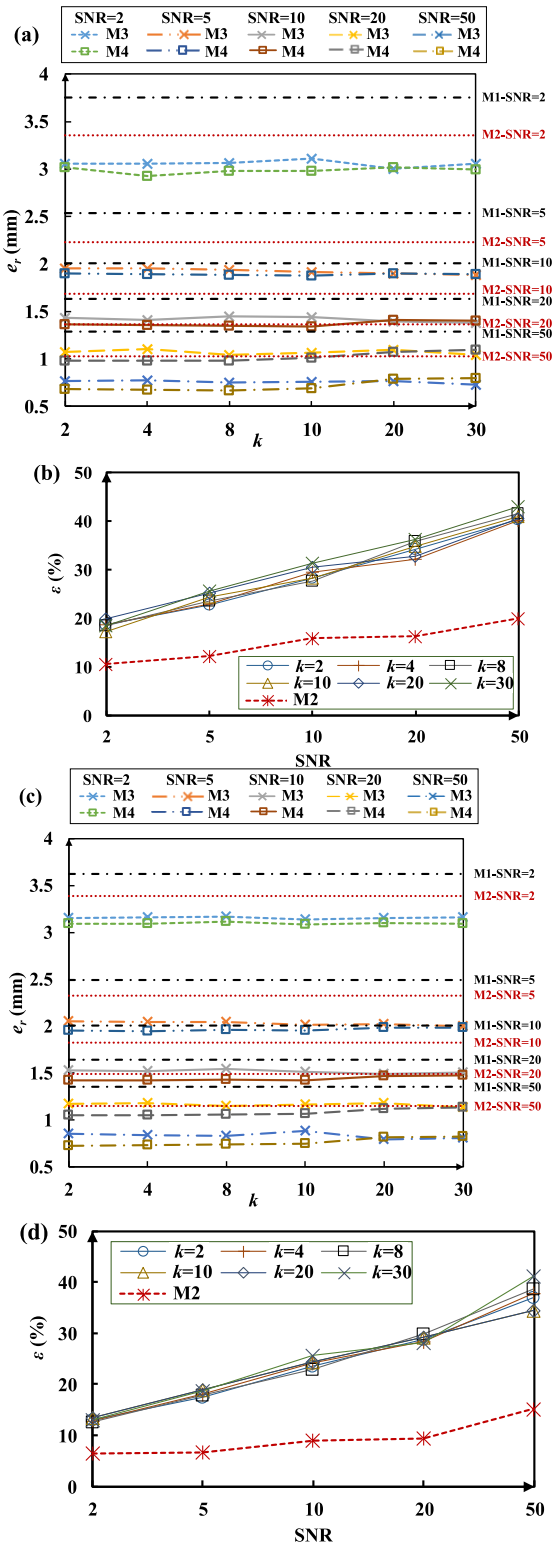

FIGURE 9. Comparisons of the mean localization error derived by M1, M2, M3 and M4. (a) and (b) The mean localization error e_r for each method and the improvement ratio ε brought by M2 and M3 (based on different k) in T-1 tracking; (c) and (d) The mean localization error e_r for each method and the improvement ratio ε brought by M2 and M3 (based on different k) in T-2 tracking.

of algorithm M2 is the maximum both in T-1 and T-2 localization. The localization error of M3 is about two times of

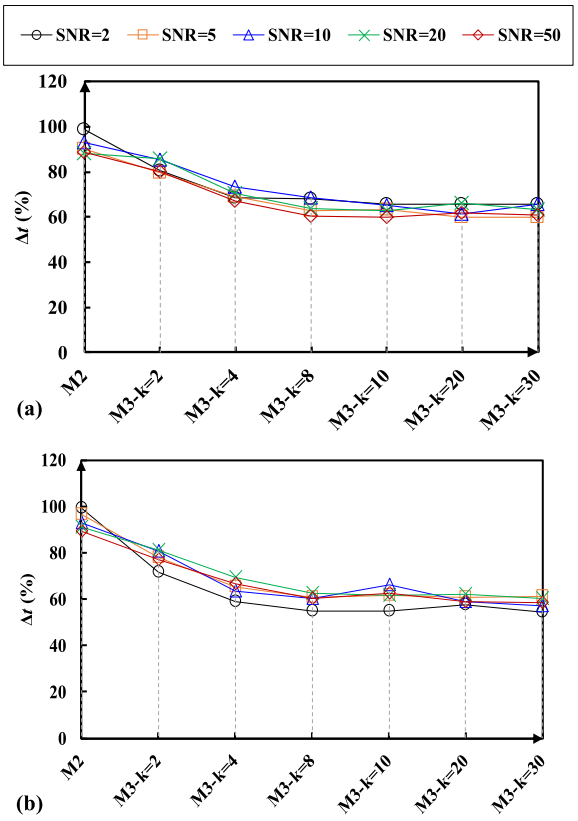

FIGURE 10. The change rates Δt for the mean processing time spent on algorithms M2 and M3 compared with M1. (a) Δt of M2 and M3 in T-1 localization; (b) Δt of M2 and M3 in T-2 localization.

M2, as presented in Figure 9. This implies the improvement brought by initial guess derived from LOMD to processing efficiency. Besides, with the node density of LOMD decrease, the processing time decreases as well between $k = 2$ to 8. This changing trend of processing time disappeared between $k = 8$ to 30, verifying that $k = 10$ is proper.

V. TEST BENCH EVALUATION

Test bench evaluations were carried out on the experiment system developed in Figure 3. Firstly, connotative pre-calibrated LOMD was constructed. Then, given trajectory was localized to assess real-time application.

A. LOMD ESTABLISHMENT

According to the extensive simulations results above, a LOMD with the weight coefficient k equals 10 is pre-calibrated by sensor array measurements. Totally, 44 nodes are involved as presented in Table 1. For each node, the PM was arranged to the planed location through control of 2-D electric linear stages according to the mechanism model in (5). Then, the immediate space MFD on the sensor array derived from the PM is recorded (sampled at 50 Hz) and utilized for (2) inverse model solving. The distributions of pre-calibrated LOMD and that computed according to the mechanism model in (5) are compared in Figure 11. The mean localization error for all LOMD nodes is 0.87 mm.

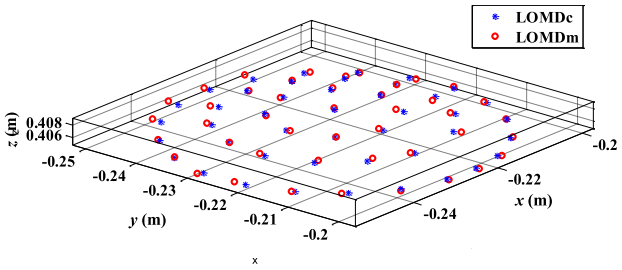

FIGURE 11. Distribution illustration of the constructed LOMD by pre-calibration (blue star) and model computation (red circle).

TABLE 2. Test bench experiment results.

Method		$\mathbf{m}$		$\mathbf{r}_p$		t	Δt
		e_θ (°)	e_φ (°)	e_r (mm)	ε (%)	(ms)	(%)
M1		2.9565	105.3281	1.3	--	11.1	--
M2		3.3373	94.4136	1.1	15.4	21.8	96.6
M3	S1 $\bar{\mathbf{m}}$	3.1604	100.6701	0.8	38.5	17.7	60.1
	S2 $\mathbf{m}'$	2.1091	46.1504				
	S3 $\mathbf{m}$	1.7842	35.3879				
M4		1.2290	20.7333	0.7	46.2	19.2	72.9

B. PERFORMANCE EVALUATION

Based on the constructed LOMD in Figure 11, a designed damped helix trace (termed T-3, illustrated in Figure 12(a)) are employed for assessment. The localization results of four methods, including the computed traces and the absolute position errors, are compared in Figures 12(b) to (e). This tracking task was repeated for 50 times. The mean orientation errors, localization errors and processing times of methods M1, M2, M3 and M4 are compared in Table 2.

The orientation errors of $\mathbf{m}$ in Table 2 show that, the deviation of φ is the largest for all four methods. This is mainly due to that the flux intensity is invariant to the rotation of the magnet along its major axis. Three kinds of orientation error during the proposed method M3 processing, which are the deviations of $\bar{\mathbf{m}}$, $\mathbf{m}'$ and $\mathbf{m}$ compared with the ideal orientation, are presented in Table 2. As illustrated in Figure 2, $\bar{\mathbf{m}}$ is the orientation result of **Step 1** with random initializations; $\mathbf{m}'$ is the LOMD searched orientation result of **Step 2** according to the preliminary localization result $\bar{\mathbf{r}}_p$; $\mathbf{m}$ is the final localization orientation result of **Step 3** with $(\bar{\mathbf{r}}_p, \mathbf{m}')$ as initialization. For method M3 in Table 2:

- The error of derived φ is larger, which attributes to that the flux intensity is invariant to the rotation of the magnet along its major axis;
- The error of $\mathbf{m}'$ in **Step 2** decreases from (3.1604 °, 100.6701 °) to (2.1091 °, 46.1504 °) compared with preliminary orientation $\bar{\mathbf{m}}$ in **Step 1**;

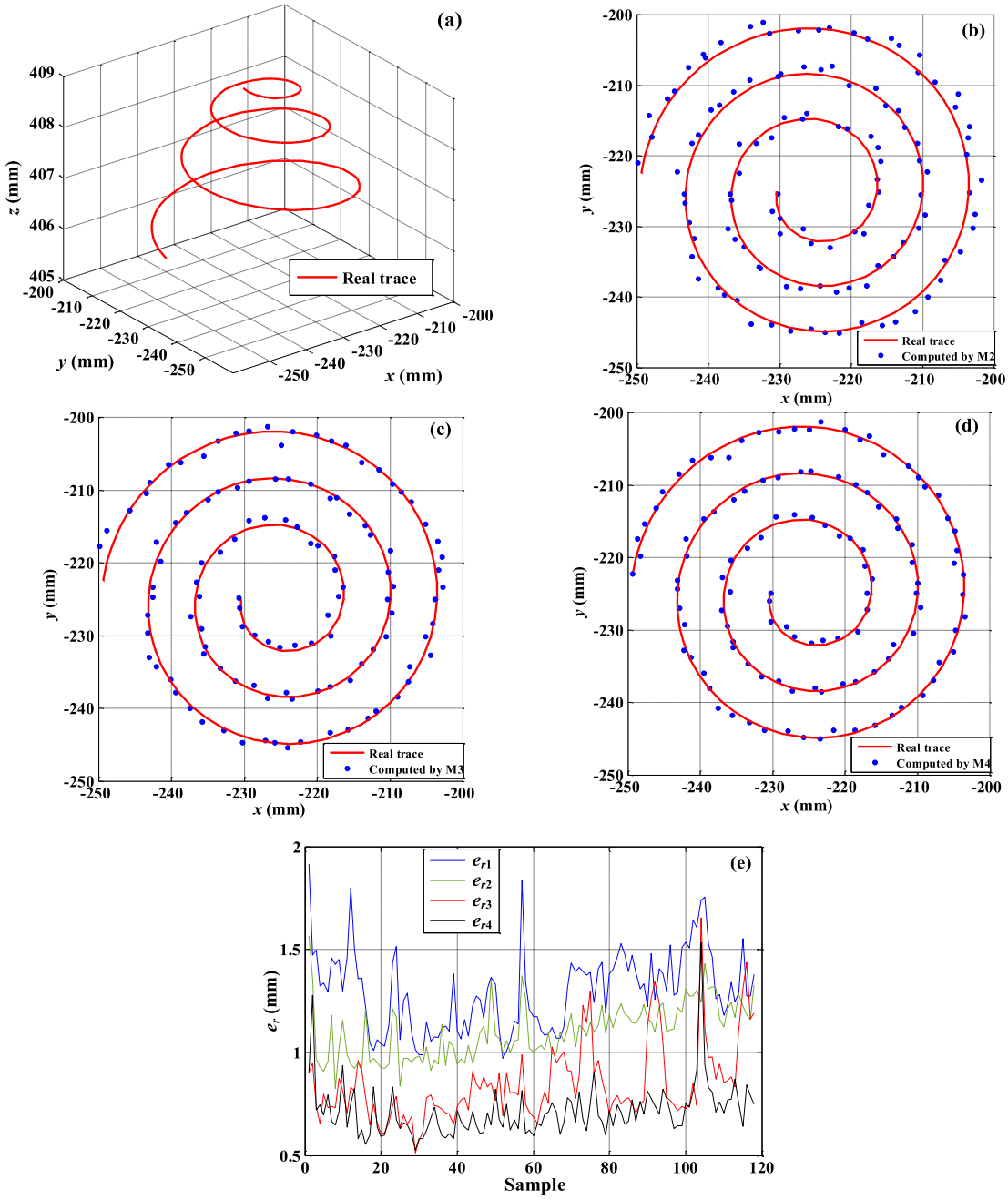

FIGURE 12. Localization error of four algorithms. (a) Illustration of the target trajectory; (b)–(c) Comparisons of real trace and that computed by method M2, M3 and M4 on the *xy*-plane; (d) Comparisons of the mean position error computed by four methods.

- The error of the final result **m** in **Step 3** is the smallest about (1.7842 °, 35.3879 °).
- The difference of both the location $\mathbf{r}_p$ and orientation **m** between methods M3 and M4 is the smallest. This validates the improvement of orientation initialization brought by the LOMD searching according to derived location parameter, which promotes the final localization.

According to the results presented in Figure 12 and Table 2, it can be observed that:

- About 38.5 % localization error improvement can be achieved by the proposed algorithm M3 compared with traditional algorithm M1;
- The mean localization error of M4 is the smallest;
- The difference between localization improvement ratio ε_3 and ε_4 is about 7.7 %, but that of processing time increase ratio is raised to 12.8 %;
- Although, the improvement of proposed method M3 is established on the cost of processing time increase from 11.1 ms (M1) to 17.7 ms (M3) with an increase ratio about 60.1 %, a real-time tracking frequency up to

56.5 Hz can be achieved. This will satisfy maximum anterior tongue movement [34].

VI. CONCLUSION

In this paper, an enhanced algorithm for real-time full-pose passive magnetic localization was presented for HMI applications, such as TMI. This algorithm combines the self-restriction that the motion of tissue and organ is muscular-skeletally restricted. The inverse magnetic localization model for the proposed magnetic marked TMI was introduced, and sensitivity of the derived MFDs to localization parameters was discussed. MFD sensitivity to position parameters, and the influence of initialization and LOMD constitution on solving the nonlinear magnetic problem were studied through extensive simulations. In test bench evaluation, a localization improvement about 38.5 % can be realized on the designed experiment system with a real-time tracking frequency up to 56.5 Hz. In the future study, adaptive method of LOMD construction with improved process efficiency and application of the proposed algorithm on the developed TMI system will be carried out.

REFERENCES

[1] N. Sebkhi, D. Desai, and M. Islam, "A multimodal speech capture system for speech rehabilitation and learning," *IEEE Trans. Biomed. Eng.*, vol. 64, no. 11, pp. 2639–2649, Nov. 2017, doi: 10.1109/TBME.2017.2654361.

[2] J. Yano, C. Shirahige, K. Oki, N. Oisaka, I. Kumakura, A. Tsubahara, and S. Minagi, "Effect of visual biofeedback of posterior tongue movement on articulation rehabilitation in dysarthria patients," *J. Oral Rehabil.*, vol. 42, no. 8, pp. 571–579, Aug. 2015.

[3] Y. K. Wang, M. P. Nash, A. J. Pullan, J. A. Kieser, and O. Röhrle, "Model-based identification of motion sensor placement for tracking retraction and elongation of the tongue," *Biomech. Model. Mechanobiol.*, vol. 12, no. 2, pp. 383–399, Apr. 2013.

[4] D. L. Adkins, J. Boychuk, M. S. Remple, and J. A. Kleim, "Motor training induces experience-specific patterns of plasticity across motor cortex and spinal cord," *J. Appl. Physiol.*, vol. 101, no. 6, pp. 1776–1782, Dec. 2006.

[5] J. L. Nuzzo, B. K. Barry, S. C. Gandevia, and J. L. Taylor, "Acute strength training increases responses to stimulation of corticospinal axons," *Med. Sci. Sports Exercise*, vol. 48, no. 1, pp. 139–150, Jan. 2016, doi: 10.1249/mss.0000000000000733.

[6] Q. Liu, G. Qian, W. Meng, Q. Ai, C. Yin, and Z. Fang, "A new IMMU-based data glove for hand motion capture with optimized sensor layout," *Int. J. Intell. Robot Appl.*, vol. 3, no. 1, pp. 19–32, Mar. 2019, doi: 10.1007/s41315-019-00085-4.

[7] E. Andrenelli, E. Ippoliti, and M. Coccia, "Features and predictors of activity limitations and participation restriction 2 years after intensive rehabilitation following first-ever stroke," *Eur. J. Phys. Rehabil. Med.*, vol. 5, no. 51, pp. 575–585, Oct. 2015.

[8] G. Yang, J. Deng, G. Pang, H. Zhang, J. Li, B. Deng, Z. Pang, J. Xu, M. Jiang, P. Liljeberg, H. Xie, and H. Yang, "An IoT–enabled stroke rehabilitation system based on smart wearable armband and machine learning," *IEEE J. Transl. Eng. Health Med.*, vol. 6, 2018, Art. no. 2100510, doi: 10.1109/jtehm.2018.2822681.

[9] Z. Pang, G. Yang, R. Khedri, and Y.-T. Zhang, "Introduction to the special section: Convergence of automation technology, biomedical engineering, and health informatics toward the healthcare 4.0," *IEEE Rev. Biomed. Eng.*, vol. 11, pp. 249–259, 2018, doi: 10.1109/rbme.2018.2848518.

[10] F. Chen, H. Lv, Z. Pang, J. Zhang, Y. Hou, Y. Gu, H. Yang, and G. Yang, "WristCam: A wearable sensor for hand trajectory gesture recognition and intelligent human-robot interaction," *IEEE Sensors J.*, vol. 19, no. 19, pp. 8441–8451, Oct. 2019, doi: 10.1109/jsen.2018.2877978.

[11] H.-M. Shen, Y. Yue, C. Lian, D. Ge, and G. Yang, "Tongue-computer interface prototype design based on t–type magnet localization for smart environment control," *Appl. Sci.*, vol. 8, no. 12, p. 2498, Dec. 2018.

[12] Y. Xin, Y. Cao, Z. Liu, Y. Chen, L. Cui, Y. Zhu, H. Hou, G. Zhao, and M. Wang, "Automatic tongue verification based on appearance manifold learning in image sequences for the Internet of medical things platform," *IEEE Access*, vol. 6, pp. 43885–43891, 2018, doi: 10.1109/access.2018.2859913.

[13] C. He, P. Kazanzides, H. Sen, S. Kim, and Y. Liu, "An inertial and optical sensor fusion approach for six degree-of-freedom pose estimation," *Sensors*, vol. 15, no. 7, pp. 16448–16465, Jul. 2015, doi: 10.3390/s150716448.

[14] I. Umay, B. Fidan, and B. Barshan, "Localization and tracking of implantable biomedical sensors," *Sensors*, vol. 3, no. 17, p. 583, Mar. 2017, doi: 10.3390/s17030583.

[15] M. N. Sahadat, N. Sebkhi, D. Anderson, and M. Ghovanloo, "Optimization of tongue gesture processing algorithm for standalone multimodal tongue drive system," *IEEE Sensors J.*, vol. 19, no. 7, pp. 2704–2712, Apr. 2019, doi: 10.1109/jsen.2018.2887257.

[16] X. Huo, J. Wang, and M. Ghovanloo, "A magneto–inductive sensor based wireless tongue–computer interface," *IEEE Trans. Neural Syst. Rehabil. Eng.*, vol. 16, no. 5, pp. 497–504, Oct. 2008, doi: 10.1109/tnsre.2008.2003375.

[17] H. A. Caltenco, B. Breidegard, and L. N. S. Andreasen Struijk, "On the tip of the tongue: Learning typing and pointing with an intra-oral computer interface," *Disab. Rehabil., Assistive Technol.*, vol. 9, no. 4, pp. 307–317, Jul. 2014, doi: 10.3109/17483107.2013.823629.

[18] A. Struijk, B. Bentsen, M. Gaihede, and E. R. Lontis, "Error–free text typing performance of an inductive intra–oral tongue computer interface for severely disabled individuals," *IEEE Trans. Neural Syst. Rehabil. Eng.*, vol. 25, no. 11, pp. 2094–2104, Nov. 2017, doi: 10.1109/tnsre.2017.2706524.

[19] X. Huo and M. Ghovanloo, "Evaluation of a wireless wearable tongue-computer interface by individuals with high-level spinal cord injuries," *J. Neural Eng.*, vol. 7, no. 2, Apr. 2010, Art. no. 026008, doi: 10.1088/1741-2560/7/2/026008.

[20] J. Kim, H. Park, J. Bruce, D. Rowles, J. Holbrook, B. Nardone, D. P. West, A. Laumann, E. J. Roth, and M. Ghovanloo, "Assessment of the tongue–drive system using a computer, a smartphone, and a powered–wheelchair by people with tetraplegia," *IEEE Trans. Neural Syst. Rehabil. Eng.*, vol. 24, no. 1, pp. 68–78, Jan. 2016, doi: 10.1109/tnsre.2015.2405072.

[21] K. Bai and K.-M. Lee, "Direct field–feedback control of a ball-joint-like permanent–magnet spherical motor," *IEEE/ASME Trans. Mechatronics*, vol. 19, no. 3, pp. 975–986, Jun. 2014, doi: 10.1109/tmech.2013.2264565.

[22] C. Hu, M.-H. Meng, and M. Mandal, "A linear algorithm for tracing magnet position and orientation by using three–axis magnetic sensors," *IEEE Trans. Magn.*, vol. 43, no. 12, pp. 4096–4101, Dec. 2007, doi: 10.1109/tmag.2007.907581.

[23] J. Lu, M. Xiao, C. Zhang, and Z. He, "Robust and fast magnetic dipole localization with singular value truncated SDM," *IEEE Access*, vol. 7, pp. 94300–94309, 2019, doi: 10.1109/access.2019.2928036.

[24] S. Song, X. Qiu, J. Wang, and M. Q.-H. Meng, "Design and optimization strategy of sensor array layout for magnetic localization system," *IEEE Sensors J.*, vol. 17, no. 6, pp. 1849–1857, Mar. 2017, doi: 10.1109/jsen.2017.2652470.

[25] D. Son, S. Yim, and M. Sitti, "A 5-D localization method for a magnetically manipulated untethered robot using a 2-D array of Hall–effect sensors," *IEEE/ASME Trans. Mechatronics*, vol. 21, no. 2, pp. 708–716, Apr. 2016, doi: 10.1109/tmech.2015.2488361.

[26] S. Song, B. Li, W. Qiao, C. Hu, H. Ren, H. Yu, Q. Zhang, M. Q.-H. Meng, and G. Xu, "6-D magnetic localization and orientation method for an annular magnet based on a closed–form analytical model," *IEEE Trans. Magn.*, vol. 50, no. 9, pp. 1–11, Sep. 2014, doi: 10.1109/tmag.2014.2315592.

[27] H.-M. Shen, L. Hu, L.-H. Qin, and X. Fu, "Real–time orientation–invariant magnetic localization and sensor calibration based on closed–form models," *IEEE Magn. Lett.*, vol. 6, pp. 1–4, 2015, doi: 10.1109/lmag.2015.2460211.

[28] C. Di Natali, M. Beccani, N. Simaan, and P. Valdastri, "Jacobian–based iterative method for magnetic localization in robotic capsule endoscopy," *IEEE Trans. Robot.*, vol. 32, no. 2, pp. 327–338, Apr. 2016, doi: 10.1109/tro.2016.2522433.

[29] J. Lim and K.-M. Lee, "Distributed multilevel current models for design analysis of electromagnetic actuators," *IEEE/ASME Trans. Mechatronics*, vol. 20, no. 5, pp. 2413–2424, Oct. 2015, doi: 10.1109/tmech.2014.2382532.

[30] Y. Higuchi, T. Nara, and S. Ando, "Complete set of partial differential equations for direct localization of a magnetic dipole," *IEEE Trans. Magn.*, vol. 52, no. 5, May 2016, Art. no. 4000910, doi: 10.1109/tmag.2015.2512536.
[31] H.-M. Shen, D. Ge, C. Lian, and Y. Yue, "Real–time passive magnetic localization based on restricted kinematic property for tongue-computer-interface," in *Proc. IEEE/ASME Int. Conf. Adv. Intell. Mechatronics (AIM)*, Hong Kong, Jul. 2019.
[32] A. Ranganath, "The levenberg-marquardt algorithm," *Tutoral LM Algorithm*, vol. 11, no. 1, pp. 101–110, Jun. 2004.
[33] C. Hu, S. Song, X. Wang, M. Q.-H. Meng, and B. Li, "A novel positioning and orientation system based on three–axis magnetic coils," *IEEE Trans. Magn.*, vol. 48, no. 7, pp. 2211–2219, Jul. 2012, doi: 10.1109/tmag.2012.2188537.
[34] C. Cheng, X. Huo, and M. Ghovanloo, "Towards a magnetic localization system for 3-D tracking of tongue movements in speech-language therapy," in *Proc. Annu. Int. Conf. IEEE Eng. Med. Biol. Soc.*, Sep. 2009, doi: 10.1109/iembs.2009.5334058.

HUI-MIN SHEN received the Ph.D. degree from the Department of Mechanical Engineering, Zhejiang University, Hangzhou, China, in 2015.

She is currently a Lecturer with the School of Mechanical Engineering, University of Shanghai for Science and Technology (USST), Shanghai, China. She is also with the State Key Laboratory of Fluid Power and Mechatronic Systems, Zhejiang University. Her research interests include magnetic signal sensing, biomedical engineering, and biomechatronics.

DI GE received the B.S. degree in material forming and control engineering from Sanjiang University, Nanjing, Jiangsu, China, in 2018. He is currently pursuing the M.S. degree in mechanical engineering with the University of Shanghai for Science and Technology, Shanghai, China.

CHONG LIAN received the B.S. degree in mechatronic engineering from Hainan University, Haikou, Hainan, China, in 2018. He is currently pursuing the M.S. degree in mechanical engineering with the University of Shanghai for Science and Technology, Shanghai, China.

YANG YUE received the B.S. degree in mechanical engineering from the Tianhua Collage, Shanghai Normal University, Shanghai, China, in 2016. She is currently pursuing the M.S. degree in mechanical engineering with the University of Shanghai for Science and Technology, Shanghai.